The Astrophysical Journal, 973:169 (11pp), 2024 October 1 https://doi.org/10.3847/1538-4357/ad6767

MOSEL Survey: Spatially Offset Lyman-continuum Emission in a New Emitter at $z = 3.088$ Can Explain the Low Number Density of Observed LyC Leakers

Anshu Gupta[1,2], Cathryn M. Trott[1,2], Ravi Jaiswar[1,2], E. V. Ryan-Weber[2,3], Andrew J. Bunker[4], Ayan Acharyya[5], Alex J. Cameron[4], Ben Forrest[6], Glenn G. Kacprzak[2,7], Themiya Nanayakkara[2,3], Kim-Vy Tran[2,8,9], and Aman Chokshi[2,10]

[1] International Centre for Radio Astronomy Research (ICRAR), Curtin University, Bentley, WA, Australia
[2] ARC Centre of Excellence for All Sky Astrophysics in 3 Dimensions (ASTRO 3D), Australia
[3] Centre for Astrophysics and Supercomputing, Swinburne University of Technology, Hawthorn, VIC 3122, Australia
[4] Department of Physics, University of Oxford, Denys Wilkinson Building, Keble Road, Oxford OX1 3RH, UK
[5] Department of Physics and Astronomy, Johns Hopkins University, Baltimore, MD 21218, USA
[6] Department of Physics and Astronomy, University of California Davis, One Shields Avenue, Davis, CA 95616, USA
[7] Swinburne University of Technology, Hawthorn, VIC 3122, Australia
[8] School of Physics, University of New South Wales, Sydney, NSW 2052, Australia
[9] Center for Astrophysics | Harvard & Smithsonian, Cambridge, MA, USA
[10] The University of Melbourne, School of Physics, Parkville, VIC 3010, Australia
Received 2024 March 17; revised 2024 July 16; accepted 2024 July 23; published 2024 September 30

Abstract

We present the discovery of a unique Lyman-continuum (LyC) emitter at $z = 3.088$. The LyC emission was detected using the Hubble Space Telescope WFC3/UVIS F336W filter, covering a rest-frame wavelength range of 760–900 Å. The peak signal-to-noise ratio of LyC emission is 3.9 in an $r = 0\farcs24$ aperture and is spatially offset by $0\farcs29 \pm 0\farcs04$ ($\sim 2.2 \pm 0.3$ kpc) from the peak of rest-UV emission (F606W). By combining imaging and spectroscopic data from the James Webb Space Telescope (JWST) JADES, FRESCO, and JEMS surveys, along with VLT/MUSE data from the MXDF survey, we estimate that the probability of random alignment with an interloper galaxy causing the LyC emission is less than 6×10^{-5}. The interstellar medium (ISM) conditions in the galaxy are similar to those in other LyC emitters at high redshift ($12 + \log(\mathrm{O/H}) = 7.79^{+0.06}_{-0.05}$, $\log U = -3.27^{+0.14}_{-0.12}$, $\mathrm{O32} = 0.63 \pm 0.03$), although the single-peaked Lyα profile and lack of rest-UV emission lines suggest an optically thick ISM. Our observations indicate that LyC photons are leaking through a narrow cone of optically thin neutral ISM, most likely created by a past merger (as evidenced by medium-band F210M and F182M images). Using the constraints on escape fraction from individual leakers and a simple model, we estimate that the opening half-angle of ionization cones can be as small as 16° (2% ionized fraction) to reproduce some of the theoretical constraints on the average escape fraction for galaxies. The narrow opening angle required can explain the low number density of confirmed LyC leakers.

Unified Astronomy Thesaurus concepts: Emission line galaxies (459); Galaxy evolution (594); High-redshift galaxies (734); Lyman-alpha galaxies (978)

1. Introduction

Understanding the escape of ionizing photons from the first galaxies remains one of the biggest challenges for models of galaxy formation and evolution. The past year of operations by the James Webb Space Telescope (JWST) has significantly transformed our understanding of galaxies in the early Universe. Nevertheless, the high opacity of the intergalactic medium (IGM) prevents us from detecting the ionizing photons escaping from the first galaxies. Therefore, we need to rely on analogs of first galaxies to understand the mode of Lyman-continuum (LyC) escape.

In the past decade, photometric observations revealed elevated emission line equivalent widths (EWs) for $z > 6$ galaxies (Labbé et al. 2013; Roberts-Borsani et al. 2016; Barro et al. 2019; Mainali et al. 2019; Endsley et al. 2020). Recent observations with JWST have confirmed this, demonstrating that 80%–90% of galaxies within the first billion years of the Universe have [O III] 5007 + Hβ EW > 800 Å, almost three times the EW of a typical star-forming galaxy at $z \sim 2$ (Cameron et al. 2023; Endsley et al. 2023; Rinaldi et al. 2023; Tang et al. 2023; Boyett et al. 2024). Consequently, many observational programs focus on studying the detailed properties of extreme emission line galaxies (EELGs), where emission lines from gas contribute almost 40%–50% to the total flux in certain photometric bands, at both low (Yang et al. 2017b; Izotov et al. 2018; Yuma et al. 2019; Lumbreras-Calle et al. 2022) and high redshifts (Atek et al. 2011; Maseda et al. 2014; Gupta et al. 2022; Davis et al. 2023; Boyett et al. 2024; Llerena et al. 2024). EELGs typically exhibit high specific star formation rates (SFRs) and high ionization parameters (Tang et al. 2019; Gupta et al. 2022; Boyett et al. 2024) that could be linked with a high LyC escape fraction (Izotov et al. 2018).

Observations of dwarf star-forming galaxies (SFGs) in the nearby Universe with Hubble Space Telescope (HST) Cosmic Origin Spectrograph have built a sizable population of local LyC leakers (Izotov et al. 2016a, 2016b, 2018; Flury et al. 2022a). The escape fraction shows a weak positive correlation with [O III] 5007/[O II] 3727 ratio and an inverse correlation with the velocity separation between the blue and red peaks of the Lyα emission (Izotov et al. 2018; Flury et al. 2022b). These observations suggest that a harder ionizing field and/or a low

covering fraction of neutral gas are crucial to facilitate the leakage of LyC photons.

At $z \sim 1$–3, the stacking experiments with SFGs yield an escape fraction of $f_{\rm esc} = 1\%$–10% (Steidel et al. 2018; Wang et al. 2023). The individual detection of LyC leakers at high redshifts is complicated by the higher chance of contamination from interloper galaxies (Vanzella et al. 2010, 2012) and attenuation by the partially neutral IGM (Inoue et al. 2014; Bassett et al. 2021). Deep imaging campaigns with HST and *u*-band imaging on ground-based telescopes have created significant samples of candidate LyC leakers at cosmic noon (e.g., Meštrić et al. 2020; Kerutt et al. 2024). Recently, Wang et al. (2023) used deep UVIS imaging from the UVCANDELS survey to report a tentative discovery of five LyC leakers at redshift $2.4 < z < 3.7$, some of them showing $f_{\rm esc} > 60\%$. However, follow-up spectroscopy is required to rule out any possible foreground contaminant.

A2218-Flanking and the Sunburst Arc are two gravitationally lensed LyC leakers at $z \sim 2.5$. In A2218-Flanking, LyC radiation is leaking from a compact dwarf galaxy (Bian et al. 2017), whereas in the Sunburst Arc, LyC radiation is leaking from a compact star-forming region that could be a young massive star cluster (Rivera-Thorsen et al. 2019). Ion1 (Vanzella et al. 2012; Ji et al. 2020), Ion2 (de Barros et al. 2016; Vanzella et al. 2016, 2020), Ion3 (Vanzella et al. 2018, 2020), and Q1549-C25 (Shapley et al. 2016) are a few examples of nonlensed LyC leakers, each showing a wide array of interstellar medium (ISM) conditions and escape fractions. For some of these galaxies, escape fractions can be higher than 50% (de Barros et al. 2016; Vanzella et al. 2016; Marques-Chaves et al. 2022; Rivera-Thorsen et al. 2022; Saxena et al. 2022). Recently, Kerutt et al. 2024 discovered five new LyC leakers using the MUSE-Wide survey (Bacon et al. 2023) by searching for LyC emission within a small aperture ($0\farcs35$) spatially coincident with peak rest-UV emission in Lyα emitters.

The Lyα emission profile for high-redshift LyC leakers exhibits a range, contrary to the classic double-peaked Lyα emission observed in most LyC leakers at $z \sim 0$. A few LyC emitters show 3–4 peaks in Lyα emission, indicative of multiple kinematic components in the neutral ISM (Vanzella et al. 2020). Lyα emission is only single-peaked in Q1549-C25 (Shapley et al. 2016) and appears in absorption in Ion1 ($z = 3.78$), indicative of a highly optically thick ISM (Ji et al. 2020). For Ion1, the LyC emission is spatially offset by $0\farcs12 \pm 0\farcs03$ from the peak UV emission, suggesting that the ionizing photons might be leaking from a small part of the galaxy. Kerutt et al. (2024) find a huge scatter between the properties of Lyα emission and escape fraction for high-redshift LyC emitters.

This paper reports the discovery of a new LyC leaker at $z = 3.088$ in the Chandra Deep Field South (CDFS, Giacconi et al. 2002) and analyzes its ISM conditions using the wealth of ancillary data from the JWST and MUSE spectrograph (Bacon et al. 2023; Bunker et al. 2023). The paper is organized as follows. Section 2 describes the photometric and spectroscopic data analyzed here. In Sections 3.1 and 3.2, we discuss the spectral energy distribution fitting, the LyC detection, and measurements of escape fraction. In Sections 3.4 and 3.5, we report properties of ISM derived from JWST/NIRSpec and MUSE spectra respectively. We discuss our results in Section 4 and present a simple model to derive the opening angle of the ionization cone. The paper uses a flat ΛCDM cosmology with $H_0 = 70$ km s^{-1} Mpc^{-1}, $\Omega_{\rm M} = 0.3$, and $\Omega_\Lambda = 0.7$.

2. Data

The galaxy z19863 (R.A. = $53\fdg1699$, decl. = $-27\fdg7684$) was identified as an EELG by Forrest et al. (2018) using photometric data from the FourStar Galaxy Evolution survey (ZFOURGE; Straatman et al. 2016). It is part of the Multi-Object Spectroscopy of Emission Line (MOSEL; Tran et al. 2020; Gupta et al. 2022) survey of galaxies, with aims to analyze the properties of EELGs at $2.5 < z < 4$. The galaxy lies in the Hubble Ultra Deep Field, providing us access to a multitude of ancillary data from both HST and JWST (Figure 1).

We combine NIRCam imaging from the JWST Advanced Deep Extragalactic Survey (JADES, Bunker et al. 2023; Eisenstein et al. 2023; Hainline et al. 2024; Rieke & the JADES Collaboration 2023), the FRESCO survey (Oesch et al. 2023), and the JWST Extragalactic Medium-band Survey (JEMS, Williams et al. 2023), giving us extensive broadband and medium-band coverage. Additionally, the FRESCO survey has released astrometrically aligned mosaics based on the archival photometry on the Hubble Legacy Fields including the UVIS/F336W imaging (Illingworth et al. 2016; Whitaker et al. 2019).

The galaxy has a spectroscopic redshift of $z = 3.088$ determined from the deep NIRSpec spectrum from JADES (Bunker et al. 2023). We also use the data from the MUSE Extremely Deep Field (MXDF, Bacon et al. 2023) to rule out interloper galaxies and analyze the Lyα emission profile. At $z = 3.088$, the UVIS/F336W filter covers rest-frame wavelengths between 760 and 900 Å, and therefore should have no contamination from nonionizing photons.

3. Analysis

3.1. Spectral Energy Distribution

We convolve the images down to a common point-spread function (PSF) of the NIRCam/F444W filter and use a 3σ threshold to create a segmentation map based on the F444W image. The fluxes are extracted within an aperture defined by KRON parameters of 2.0. A slightly lower KRON parameter is used here to minimize the contamination from a nearby background source at $z = 3.4$. We estimate errors by taking the rms of flux at random locations within the same aperture for each image.

We use the MAGPHYS (da Cunha et al. 2008, 2015) spectral energy distribution (SED) fitting code with the BC03 stellar population synthesis model (Bruzual & Charlot 2003), the delayed exponentially declining star formation history model, and the Charlot & Fall (2000) dust attenuation law to derive physical properties. We only use filters that are not contaminated by bright nebular emission lines such as [O III] 5007 and Hα (all except F210M and F277W, Figure 2). We also do not include an IGM absorption model. Refer to Table 1 to check the results from the SED fitting.

3.2. LyC Detection

We use the HST UVIS/F336W mosaics released by the FRESCO survey (Oesch et al. 2023), which were created using the Hubble Legacy Fields photometry (Teplitz et al. 2013; Rafelski et al. 2015; Illingworth et al. 2016; Whitaker et al. 2019),

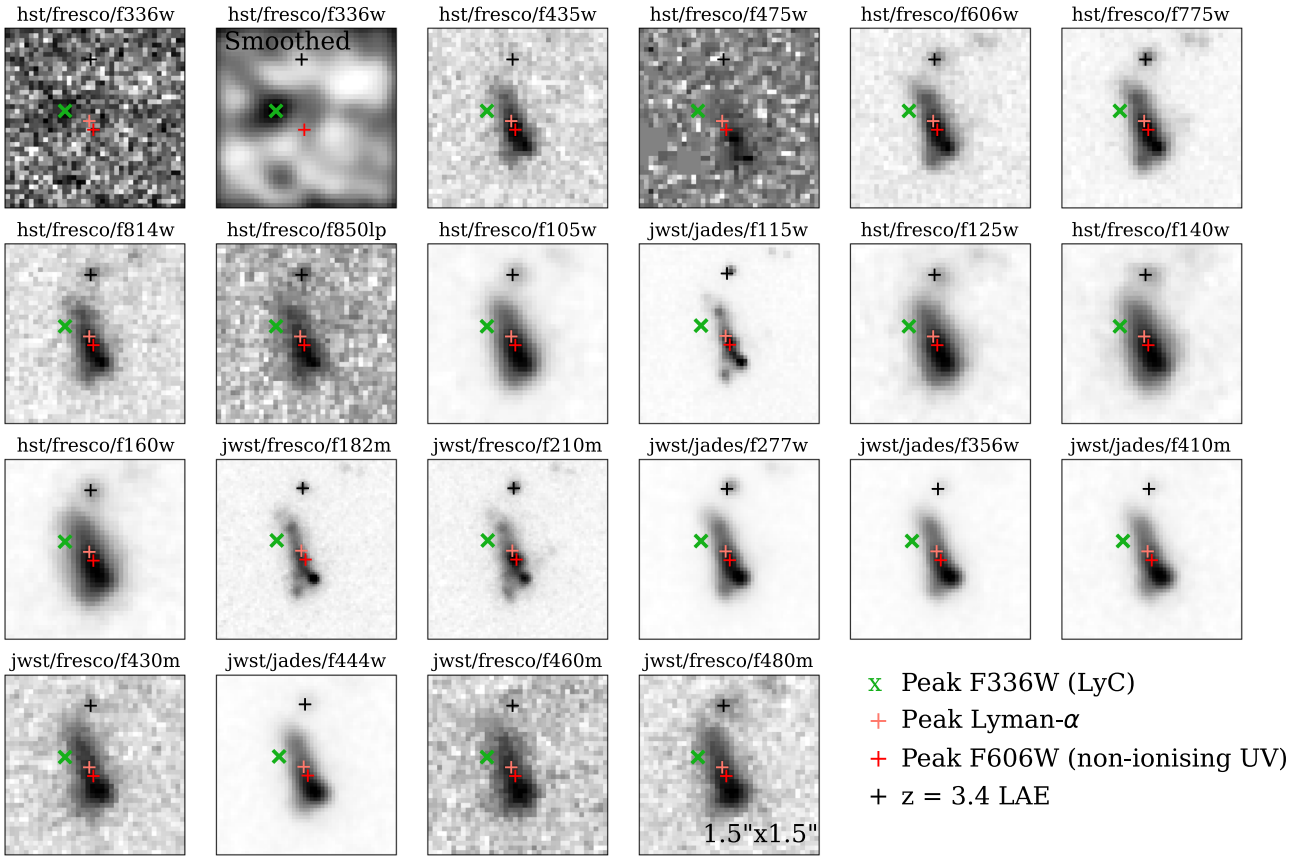

Figure 1. Multiband imaging of galaxy z19863 from HST and JWST in increasing order of wavelength. Each panel is $1\farcs5 \times 1\farcs5$ across. The top two panels correspond to the original and PSF-smoothed images from the HST F336W filter (LyC). The red plus, salmon plus, and green cross mark the positions of the nonionizing rest-UV (F606W), Lyα emission, and ionizing rest-UV (F336W) peaks, respectively. The black plus marks the location of the $z = 3.4$ Lyα emitter detected in the MXDF survey (see Section 3.5) for more details.

to visually search for LyC emission around MOSEL targets. The mosaic relies on the archival HST imaging and hence has nonuniform coverage and depth across the FRESCO field of view (FOV). Out of 76 EELGs identified by Forrest et al. (2018) in the CDFS, 54 fall within the FRESCO FOV. We only found significant emission around one EELGs that happened to fall in the deepest region in the F336W image. Figure 1 shows the multiband imaging for z19863, along with the unconvolved and PSF-convolved F336W imaging, clearly indicating the possible LyC emission toward the NE side of the galaxy.

We estimate the signal-to-noise ratio (SNR) of LyC emission by placing an aperture of variable size at the pixel corresponding the peak emission in both the unconvolved and PSF-convolved F336W images (Figure 3). In the unconvolved image, we reach a maximum SNR of 4.0 within an aperture of $r = 0\farcs12$, corresponding to $m_{\rm F336W} = 28.7^{+0.3}_{-0.2}$. The SNR drops marginally to 3.95 at $r = 0\farcs24$, corresponding to $m_{\rm F336W} = 27.9^{+0.3}_{0.2}$, a slightly larger aperture size than the FWHM ($0\farcs17$) of the F336W filter. The SNR drops to 2.4 at $r = 0\farcs32$ and results in a marginal drop in flux ($m_{\rm F336W} = 28.0^{+0.4}_{-0.3}$). In the PSF-convolved image, the SNR reaches a maximum of 3.3 within an aperture of $r = 0\farcs2$. The PSF-convolved image does indicated some weak evidence of extended LyC emission. Using an elliptical aperture ($a = 0\farcs28$, $b/a = 0.7$, $\theta = 120°$), results in only a marginal increase in the SNR; therefore, significant flux is not lost by the choice of a circular aperture.

3.2.1. Detection Reliability Test

To test the reliability of our detection, we check for the growth curve at random locations in the $1' \times 1'$ region covering the deepest F336W data. We use the F160W segmentation map to mask out all bright targets in the F336W image. We then place two circular apertures of $r = 0\farcs12$ and $0\farcs24$ at 20,000 random locations. We only measured the growth curve if the percentage of unmasked pixels within the largest aperture was greater than 90%. Only one random location out of nearly 16,470 possible locations had SNR $\geqslant 4.0$ within aperture $r = 0\farcs12$ and SNR $\geqslant 3.9$ within aperture $r = 0\farcs24$. There is clear emission in the F606W image at the same random location, indicating that the false detection is an interloper galaxy. We do not detect any signature of any interlopers in either HST or JWST imaging or in the MUSE data cube coincident with the LyC detection. Thus the probability of randomly detecting a similar source is $p < 6 \times 10^{-5}$.

3.2.2. Spatial Offset of Ionizing Emission

The peak nonionizing UV emission (F606W) and ionizing emission have a spatial offset of $0\farcs29 \pm 0\farcs04$ or 2.2 ± 0.3 kpc at $z = 3.088$. We checked for astrometric alignment between the F336W and F606W images by estimating the difference in the centroids of the 20 brightest sources in the deepest $1' \times 1'$ FOV F336W image. The average difference in x-centroid [y-centroid] is 0 ± 1 [0 ± 1] pixels, significantly smaller than the peak separation ($\sim$7 pixels) between ionizing and nonionizing

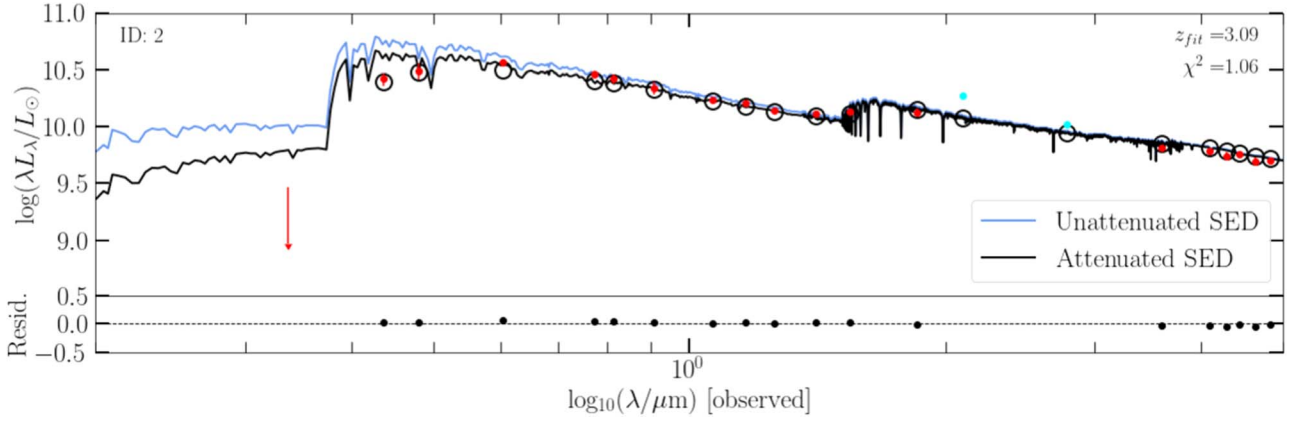

Figure 2. The best-fit SED model using MAGPHYS before (blue curve) and after (black curve) correcting for dust attenuation. The red dots and open black circles correspond to the observed flux and derived flux from the best-fit SED respectively. The cyan dots represents the two filters (F210M and F277W) that are excluded while modeling the SED to minimize contamination by bright [O III] 5007 and Hα emission lines.

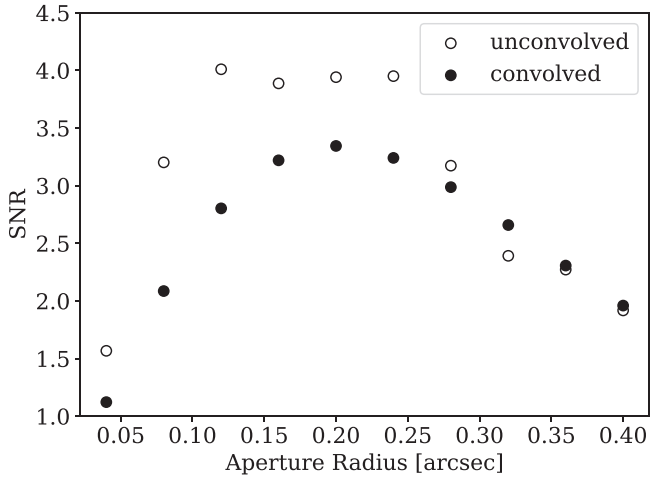

Figure 3. The SNR as a function of the aperture radius for the unconvolved (open circles) and PSF-convolved (filled circles) F336W images. Each aperture is positioned at the peak LyC flux (green cross in Figure 1).

emission from our target. Therefore, the astrometric inaccuracies cannot account for the spatial offset.

3.2.3. LyC Escape Fraction

The escape fraction is defined as the ratio of ionizing ($f_{\rm LyC}$ at $\lambda < 912$ Å) and nonionizing flux density ($f_{\rm nLyC}$ typically at 1500 Å, Steidel et al. 2001). We use the standard procedure to calculate escape fraction (e.g., Siana et al. 2007; Ji et al. 2020). As mentioned earlier, we use the F606W filter (rest frame ∼1500 Å) to measure nonionizing photon flux density. The ionizing photons can sometimes escape from certain parts of the galaxy (Verhamme et al. 2015), therefore we use the same aperture to estimate flux for both ionizing and nonionizing UV components. Using an aperture of radius $r = 0\farcs12$ centered at the peak LyC emission for both ionizing and nonionizing UV emission, we estimate $(f_{\rm LyC})_{\rm obs} = 12.5 \pm 3.1$ nJy and $(f_{\rm nLyC})_{\rm obs} = 11.7 \pm 1.2$ nJy. If we use an aperture of $r = 0\farcs24$, then $(f_{\rm LyC})_{\rm obs} = 24.5 \pm 6.2$ nJy and $(f_{\rm nLyC})_{\rm obs} = 89.9 \pm 2.5$ nJy. Thus, $(f_{\rm nLyC}/f_{\rm LyC})_{\rm obs} = 0.9 \pm 0.3$ within the $r = 0\farcs12$ aperture and $(f_{\rm nLyC}/f_{\rm LyC})_{\rm obs} = 3.7 \pm 0.9$ within the $r = 0\farcs24$ aperture. This estimate is done after convolving the F336W and F606W images to a common PSF of F606W.

Table 1
Physical Properties of z19863

R.A. [deg]	53.1699
Decl. [deg]	−27.7684
z	3.088
$\log(M_*/M_\odot)$	9.2 ± 0.1
$\rm SFR_{H\alpha}$ [$M_\odot$ yr^{-1}]	4.3 ± 0.09
$\rm SFR_{SED}$ [$M_\odot$ yr^{-1}]	5.2 ± 0.2
$E(B-V)_{\rm gas}$	0.09 ± 0.02
12 + log(O/H)	$7.79^{+0.06}_{-0.05}$
log$U$	$-3.27^{+0.14}_{-0.12}$
$L_{1500}/L_{900} = 6.66$, MAGPHYS	
$f_{\rm esc}^{\rm rel}$	2.8 ± 0.7
$f_{\rm esc}^{\rm abs}$	1.2 ± 0.3
$L_{1500}/L_{900} = 1.25$, lower limit	
$f_{\rm esc}^{\rm rel}$	0.5 ± 0.1
$f_{\rm esc}^{\rm abs}$	0.24 ± 0.06

We need precise measurements of the ratio of intrinsic nonionizing to ionizing photon luminosity (L_{1500}/L_{900}), accurate IGM attenuation ($T_{\rm IGM}$) at the redshift of our galaxy, and the dust attenuation (A_{1500}) to estimate relative and absolute escape fractions. We use the IGM transmission of $T_{\rm IGM} = 0.66$ at $z = 3.08$ calculated by Kerutt et al. (2024), which uses the mean transmission from the brightest 5% of sightlines based on the model of Inoue et al. (2014). The adopted $T_{\rm IGM}$ sits comfortably in the range calculated for $z = 3.1$ Lyα emitters by Bassett et al. (2021, see their Figure 6), taking into account the bias of detected LyC emitters along clean lines in the IGM.

Using $E(B-V) = 0.09 \pm 0.02$ (see Section 3.4.1) and the extinction curve for the Small Magellanic Cloud from Gordon et al. (2003), we obtain $A_{1500} = 1.2 \pm 0.3$. We note that the NIRSpec spectra do not cover the region where LyC emission is detected. The region occupied by the bulk of gas emitting Hα and Hβ emission lines can be different from the region with bright OB-type stars, as has been postulated by other studies (Vanzella et al. 2020, 2022; Meštrić et al. 2023). Therefore, the extinction toward the LyC region could be significantly different.

Finally, the intrinsic luminosity ratio L_{1500}/L_{900} can vary between 1.25 and 7 depending on the assumptions in the stellar population model (Leitherer et al. 1999; Eldridge et al. 2017). The best-fit SED model from MAGPHYS (Section 3.1) gives $L_{1500}/L_{900} = 6.66$, resulting in $f_{\rm esc}^{\rm rel} = 2.8 \pm 0.7$ and

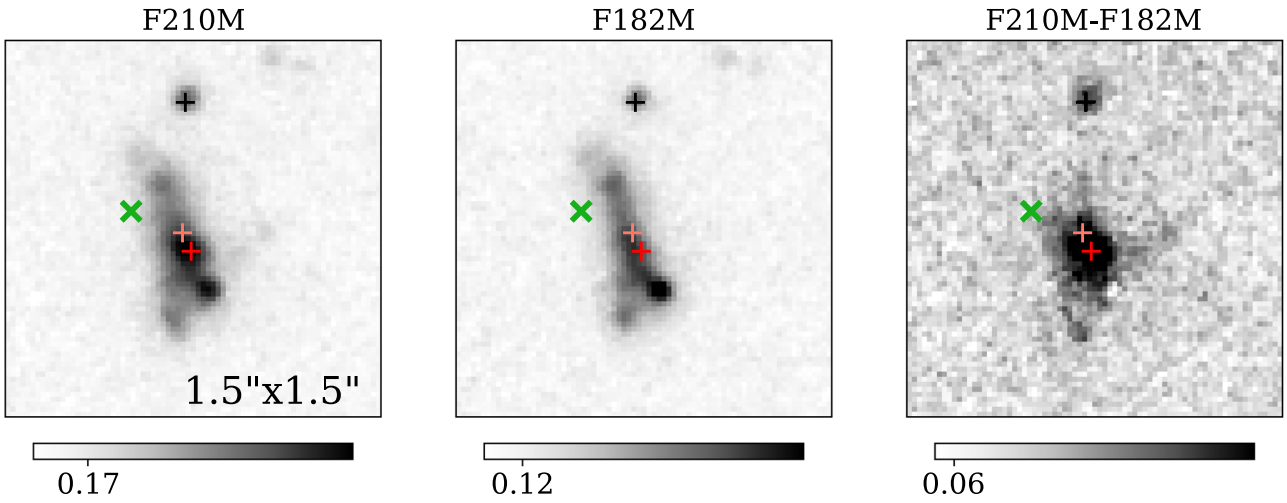

Figure 4. JWST medium-band F210M (left: stars + gas), F182M (middle: stars), and F210M – F182M (right: gas) images for the galaxy z19863 at $z = 3.088$. The overplotted symbols follow the same scheme as Figure 1.

$f_{\rm esc}^{\rm abs} = 1.3 \pm 0.3$. An escape fraction >1 is unphysical because it implies the LyC-leaking region of the galaxy is leaking more than the ionizing photons produced in this ionization cone. Note that the properties of the stellar population might not be the same throughout the galaxy: for example, the LyC-leaking region could have a significantly younger stellar population than the rest of the galaxy. Even assuming a more typically used $L_{1500}/L_{900} = 3$, we get $f_{\rm esc}^{\rm rel} = 1.2 \pm 0.3$ and $f_{\rm esc}^{\rm abs} = 0.6 \pm 0.1$. Using the lower limit on $L_{1500}/L_{900} = 1.25$ gives us the most conservative estimate of the relative escape fraction of $f_{\rm esc}^{\rm rel} = 0.5 \pm 0.1$ and a corresponding $f_{\rm esc}^{\rm abs} = 0.24 \pm 0.06$. A future paper will analyze the properties of the resolved stellar population of z19863 and test the impact that different stellar population models have on the measurements of escape fraction.

3.3. Merger Activity

We use medium-band filters F210M and F182M to analyze the merger activity of our source. At $z = 3.088$, the medium-band filter F210M would contain emission from stars and the [O III] 5007 + Hβ emission lines, whereas filter F182M would only have stellar emission. Therefore, the difference image between the two filters provides a spatially resolved distribution of gas emission ([O III] 5007 + Hβ) from the target (Figure 4). We use StatMorph (Rodriguez-Gomez et al. 2019) to estimate nonparametric quantities for all three filters (more details in A. Gupta et al. 2024, in preparation) .

The Gini-M20 statistics (Lotz et al. 2008) classify z19863 as a merger based on the stellar emission (F182M) but a non-merger based on the gas emission (F210M – F182M). The peak gas emission (F210M – F182M) is coincident with the peak nonionizing UV emission (F606W), whereas the peak stellar emission (F182M) is 0.″18 SW of the nonionizing UV emission (F606W). The lack of merger signs in the gas emission could be because hydrodynamical cooling results in faster settling for the gas than the stars after a merger event (see A. Gupta et al. 2024, in preparation for more discussion). We detect significant gas emission (F210M – F182M) coincident with the LyC peak, indicating ongoing star formation activity. However, the lack of a defined peak in gas emission suggest that LyC photons are more likely to be leaking due to an optically thin ISM rather than a peak in star formation activity at this location. A detailed analysis of spatially resolved spectral properties of z19863 is beyond the scope of this paper and will be part of future analysis

3.4. JADES/NIRSpec Observations

Figure 5 shows the JWST/NIRSpec spectrum for z19863 from JADES (NIRSpec ID = 21150, NIRCam ID = 211968; Bunker et al. 2023) spanning all the way from 1 to 5 μm and showing multiple bright emission lines. Note that the 0.″46 microshutter only partially covers the galaxy and only on the side opposite to the LyC detection. We cannot use the NIRSpec spectra to rule out the emission in the F336W image being due to an interloper galaxy. Even with this partial coverage, we are able to detect a whole suite of emission lines to estimate the gas-phase metallicity and ionization conditions in the galaxy.

The emission line fluxes in the JADES catalogs have been aperture-corrected using the location of the microshutter on the NIRCam imaging. The analysis in the following subsections assumes that the gas has similar properties across the entire galaxy, which might not be correct. Neither [N II] 6583 nor [S II] 6717, 6731 is detected at SNR > 5 with the grism, therefore we rely on the JADES prism catalogs to estimate ISM conditions.

3.4.1. Dust Extinction and Star Formation

We use the Gordon et al. (2003) extinction curve for the Small Magellanic Cloud to correct for dust extinction, following a similar approach used in previous studies of high-redshift galaxies (Cameron et al. 2023; Reddy et al. 2023). We use the Balmer decrement based on the ratio of Hα and Hβ emission lines to estimate the color excess using the equation

$$E(B-V) = \frac{2.5}{\kappa(\mathrm{H}\beta) - \kappa(\mathrm{H}\alpha)} \log_{10}\left(\frac{(\mathrm{H}\alpha/\mathrm{H}\beta)_{\rm obs}}{2.98}\right). \quad (1)$$

The Balmer decrement for z19863 is $f(\mathrm{H}\alpha/\mathrm{H}\beta)_{\rm obs} = 3.26 \pm 0.07$, which results in $E(B-V) = 0.09 \pm 0.02$.

The dust-corrected SFR based on Hα and using the Kennicutt & Evans (2012) relation is $4.3 \pm 0.09\ M_{\odot}\ \mathrm{yr}^{-1}$ for this galaxy, placing it within the main sequence at $z = 3$ (Popesso et al. 2022). It is important to note that the Hα luminosity used for this calculation is rescaled based on the

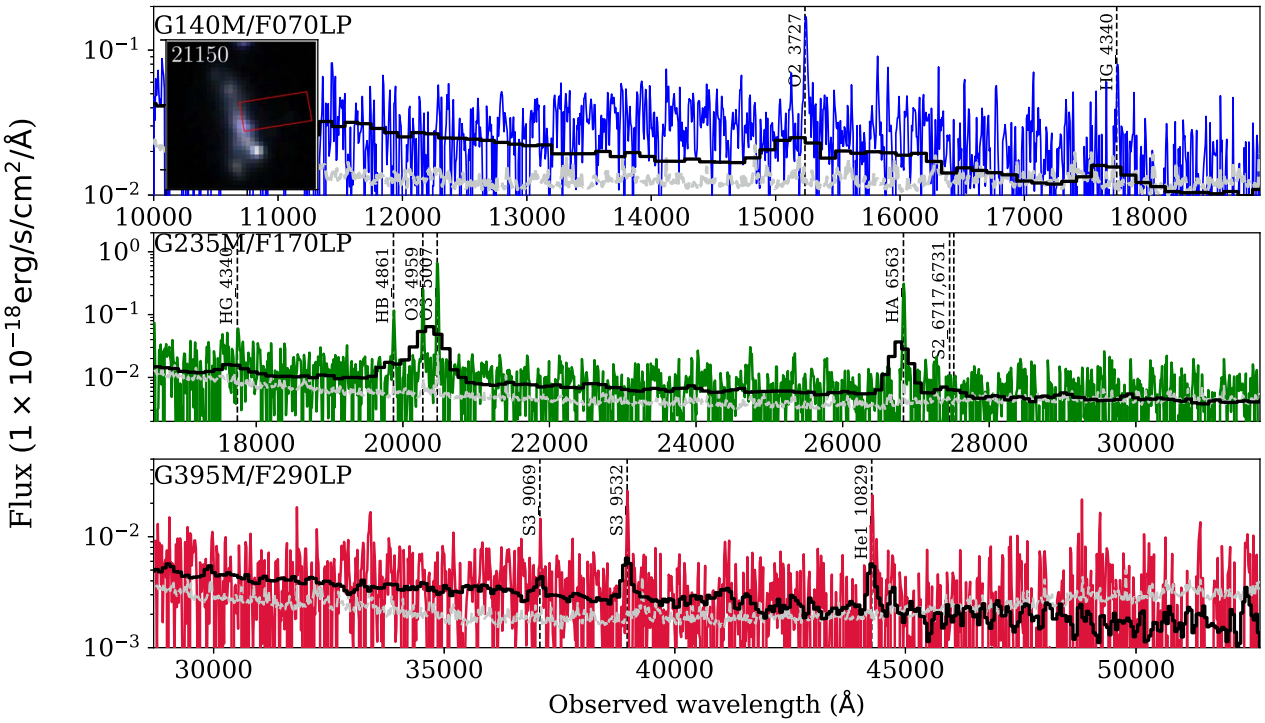

Figure 5. NIRSpec spectrum (JADES NIRSpec ID = 21150, NIRCam ID = 211968) from JADES in the three medium-band grisms, G140M/F070LP (top), G235M/F170LP (middle), and G395M/F290LP (bottom). The gray dashed curve in each panel corresponds to the error spectrum in the respective grism. The low-dispersion prism spectrum is shown as the solid black curve in each panel and has a significantly lower error spectrum than the ranges displayed here. The black dashed lines mark the location of bright emission lines detected above the 5σ level in each subpanel. The inset image in the top panel shows the location of the slit with respect to the JWST/NIRCam image (taken from Figure B.1 in Bunker et al. 2023).

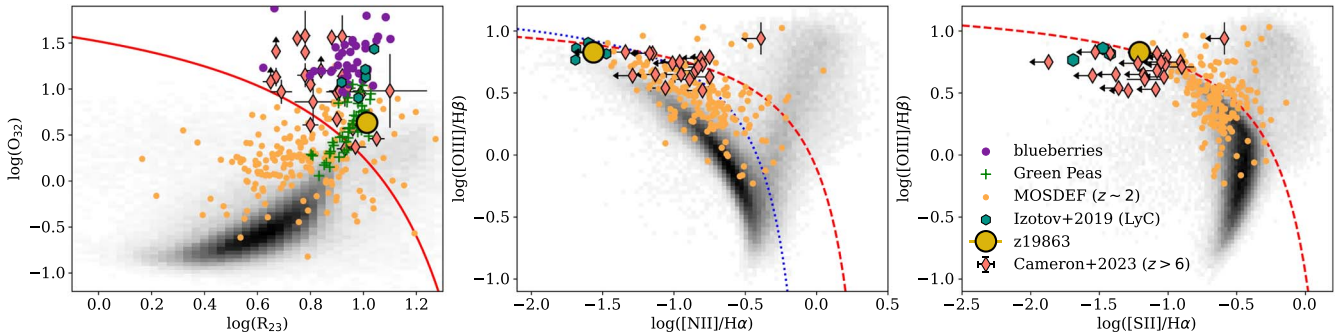

Figure 6. The location of z19863 (golden circle) on the R23 − O32 (left), N2 − R2 (middle), and S2 − R2 (right) diagrams, is typically used to probe the metallicity and ionization conditions of the ISM. The $z \sim 6$ galaxies from Cameron et al. (2023) are shown as salmon diamonds. We also compare with other extreme galaxies in the local Universe (blueberries from Yang et al. 2017a: purple circles, green peas from Yang et al. 2017b: green pluses, and LyC leakers from Izotov et al. 2018: green hexagons). The gray shaded regions and the orange dots in each panel represent the typical SFGs at $z \sim 0$ from the Sloan Digital Sky Survey (Aihara et al. 2011) and at $z \sim 2$ from the MOSDEF survey (Kriek et al. 2015) respectively. The solid red curve in the left panel and the dashed red curves in the middle and right panels show the relations of Lamareille et al. (2004) and Kewley et al. (2001) respectively for identifying active galactic nuclei. The blue dotted curve in the middle panel represents the Kauffmann et al. (2003) relation for star-forming galaxies. Our galaxy falls in the star-forming region occupied by metal-poor galaxies, similar to $z > 6$ galaxies and other extreme galaxies in the local Universe.

position of the microshutter on the NIRCam image of the galaxy. However, the pseudo [O III] 5007 emission map reveals that the microshutter misses the most star-forming part of the galaxy (Figure 4). Therefore, the total Hα luminosity and the instantaneous SFR of z19863 may differ significantly from the value estimated here.

3.4.2. Ionization Conditions

The left panel in Figure 6 displays the extinction-corrected R23 versus O32 relation of z19863 compared to those of other LyC emitter samples and galaxies at $z > 6$, where

$$\mathrm{R23} = \log_{10}((\mathrm{[O\ III]}\ 5007, 4959 + \mathrm{[O\ II]}\ 3727)/\mathrm{H}\beta),$$

$$\mathrm{O32} = \log_{10}(\mathrm{[O\ III]}\ 5007/\mathrm{[O\ II]}\ 3727).$$

To correct for dust extinction for low-redshift samples, we apply the CCM89 extinction curve ($R_V = 3.1$, Cardelli et al. 1989). The O32 (0.63 ± 0.03) and R23 (1.01 ± 0.03) ratios of z19863 are higher than those of typical star-forming galaxies both in the local Universe (Aihara et al. 2011) and at $z \sim 2$ (Shapley et al. 2014; Kriek et al. 2015). The emission line

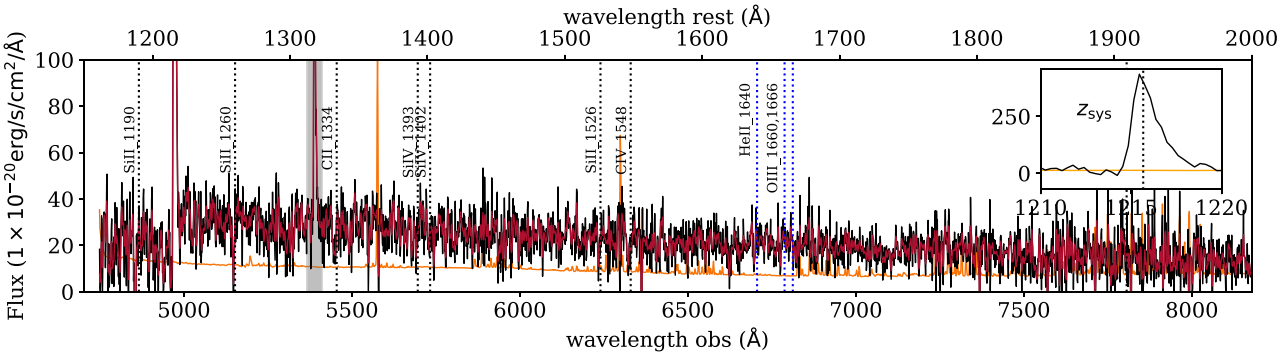

Figure 7. The black and red curves show the rest-UV 1D spectrum extracted from the MXDF mosaic (12 hr integration) before and after convolving with a Gaussian kernel of $\sigma = 1$ respectively. The inset image shows the zoomed-in spectrum at the location of the Lyα emission line. The dashed vertical lines mark the location of various absorption features. The dashed orange curve is the corresponding error spectrum. The gray shaded region highlights the Lyα emission from the nearby $z = 3.4$ galaxy.

ratios of z19863 resemble those of other extreme galaxy populations such as green peas and blueberries in the local Universe. However, its O32 ratio is not as high as that of other LyC emitters at $z \sim 0.3$. z19863 also exhibits a low S2, where

$$\mathrm{S2} = \log_{10}(([\mathrm{S\,II}]\,6717, 6731)/\mathrm{H}\alpha),$$

compared to typical star-forming galaxies at $z \sim 2$, which has also been indicated as a marker for LyC leakers (Ramambason et al. 2020).

Interestingly, we have detections of both [S III] 9069, 9531 and [S II] 6717, 6731 in the prism spectrum of z19863. Therefore, we can use the S32 ratio defined as

$$\mathrm{S32} = \log_{10}([\mathrm{S\,III}]\,9069, 9531/[\mathrm{S\,II}]\,6717, 6731)$$

to estimate the ionization parameter; it is a metallicity- and pressure-independent ionization parameter diagnostic. Traditionally, the O32 ratio is used to estimate the ionization parameter because [S III] 9069, 9531 redshifts either into the near-infrared at $z > 0.05$ or beyond 2.4 μm at $z > 1.5$, making it difficult to observe. However, ionization parameters based on O32 are highly dependent on the choice of stellar template (Sanders et al. 2015). Sanders et al. (2019) used stacked measurements of [S III] 9069, 9531 in $z \sim 1.5$ galaxies and confirmed its weaker dependence on metallicity compared to O32. Recent observations have started to use [S III] 9069, 9531 to estimate the ionization conditions in galaxies (Mingozzi et al. 2020; Kumari et al. 2021).

The S32 ratio of z19863 is 0.27 ± 0.09. Assuming $12 + \log(\mathrm{O/H}) = 7.8$, we estimate an ionization parameter of $\log U = -3.25 \pm 0.10$, similar to the ionization parameter of typical SFGs at $z \sim 2$–3 (Sanders et al. 2015), and significantly lower than for galaxies at $z > 6$. In contrast, using O32 ratio of $= 0.63 \pm 0.03$ gives $\log U = -2.44 \pm 0.03$ at the same metallicity. We suspect the difference in the ionization parameters is due to the lack of independent constraints on the gas temperature. Pérez-Montero et al. (2019) show that without accurate measurements of gas temperature, O32 alone can produce as much as 1 dex variation in the ionization parameter. Moreover, the emissions lines associated with the respective indicators originate from different parts of the nebula, and hence might be susceptible to inherent inhomogeneities.

Again, we note that NIRSpec observations only cover a small portion of the galaxy. Spatially resolved observations of star-bursting galaxies find significant variations in metallicity and ionization parameter (del Valle-Espinosa et al. 2023), indicating that NIRSpec spectra might not be representative of the average gas conditions in the galaxy.

3.4.3. Gas-phase Metallicity

The [N II] 6583 emission line is not detected in either the grism or prism spectrum, indicative of very low metallicity. We use the grism spectra to estimate an upper limit on [N II] 6583 because [N II] 6583 is blended with Hα in the prism spectrum. The [N II] 6583/Hα versus [O III] 5007/Hβ diagram (Figure 6) places the galaxy well within the region occupied by low-metallicity star-forming galaxies in both the low- and high-redshift Universe.

We use the S23 diagnostic from Kewley et al. (2019) to estimate the gas-phase metallicity, where

$$\mathrm{S23} = \log_{10}(([\mathrm{S\,II}]\,6717, 6731 + [\mathrm{S\,III}]\,9069, 9531)/\mathrm{H}\alpha),$$

due to its sensitivity at lower metallicity and the lack of [N II] 6583 detection. Using an $S23$ ratio of -0.75 ± 0.05 and $\log U = -3.25$, we estimate the gas-phase metallicity at $12 + \log(\mathrm{O/H}) = 7.79^{+0.06}_{-0.05}$ ($Z = 0.13 \pm 0.01\ Z_\odot$). Thus, the gas-phase metallicity of our galaxy is fairly consistent with gas-poor galaxies detected at higher redshifts (Tang et al. 2023; Boyett et al. 2024).

3.5. Rest-UV Spectrum

We extract the rest-UV spectrum of our target using the mosaic data cube from the MXDF survey (Bacon et al. 2023). The mosaic data cube reaches a total integration time of 12 hr at the position of our target (peak flux in F606W filter). We search for emission around the expected Lyα wavelength at $z = 3.088$, and identify the peak wavelength. We sum over flux within ± 10 Å around the peak Lyα wavelength to create a line map and add spaxels above $2 \times \mathrm{rms_{sky}}$ to extract the 1D spectrum (Figure 7).

The Lyα emission coincides with the nonionizing UV emission (F606W, $<0\farcs1$), and is highly asymmetric with an undetected blue side, similar to other high-redshift Lyα emitters (Gronke & Dijkstra 2016). The red peak of the Lyα emission has a marginal velocity offset from the systematic redshift of the galaxy (approximately 100 km s^{-1}). There is significant contamination in the rest-UV spectrum from another Lyα emitter at $z = 3.4$, which is only $0\farcs65$ from the F606W peak (indicated as a black plus in Figure 1). The high spatial

resolution of HST and JWST ensures negligible contamination in the photometry of z19863 from this source at any wavelengths including the F336W image. We have clear detections of many low-ionization (Si II λ1190, Si II λ1260, C II λ1334, Si II λ1526) and high-ionization (Si IV $\lambda\lambda$1393, 1402, C IV $\lambda\lambda$1548, 1550) metal absorption features. Interestingly, we do not detect any high-ionization emission lines such as [O III] 1660, 1666, He II 1640, [C III] 1907, 1909, which are commonly detected in other LyC emitters (Vanzella et al. 2020). Ji et al. (2020) also report a tentative detection of He II 1640 (SNR $\sim$ 2) in Ion1, indicating the need for a deeper rest-UV spectrum.

4. Discussion

4.1. Curious Case of z19863

This paper presents the discovery of a new LyC emitter candidate, z19863 at redshift $z = 3.088$, combining archival data from deep imaging campaigns conducted on the HST and JWST (Figure 1). Detailed information about the source is provided in Table 1. Using the deep NIRSpec spectrum from JADES we find that z19863 has characteristics similar to other LyC emitters across different redshift ranges (see Figure 6), including a moderate ionization parameter ($\log U = -3.25 \pm 0.1$), a low gas-phase metallicity ($12 + \log(\mathrm{O/H}) = 7.76 \pm 0.06$), and a high O32 ratio (0.63 ± 0.03). Notably, the LyC emission is spatially offset by $0\farcs29 \pm 0\farcs04$ (equivalent to 7 ± 1 pixels or approximately 2.2 kpc) from the peak rest-UV (nonionizing) emission (Figure 1). The astrometric misalignment is insufficient to account for the spatial offset ($dx = \pm 1$ pixel). We do not detect any interloper galaxy coincident with the LyC detection in extremely deep spectroscopy from the MXDF survey (Figure 7). We estimate the probability of randomly detecting a similar source within a similar aperture ($0\farcs24$) in the F336W image is $p < 6 \times 10^{-5}$.

Most observations focused on detecting LyC photons typically search for emission at $\lambda_{\mathrm{rest}} < 912$ Å cospatial with the nonionizing UV emission. For example, Kerutt et al. (2024) look for LyC emission within $0\farcs35$ aperture around the nonionizing rest-UV emission, and therefore would miss a source similar to z19863 with about $0\farcs29$ offset between the peaks of ionizing and nonionizing emission. Ion1 ($z = 3.7$) is another known LyC emitter that exhibits a spatial offset between the peak rest-UV and LyC emission ($0\farcs12 \sim 0.85$ kpc, Ji et al. 2020).

Additionally, z19863 has a single-peaked Lyα emission profile (Figure 7), which is atypical for LyC emitters in the local Universe, where a double-peaked profile with a narrow velocity separation is common (Izotov et al. 2018, 2022; Flury et al. 2022b). Models of LyC and Lyα escape suggest that a narrow velocity separation is indicative of an optically thin neutral ISM, which, in turn, facilitates the escape of ionizing photons (Izotov et al. 2018). The green pea galaxies with high O32 ratios (which are more likely to leak LyC photons) have lower H I gas mass, suggesting they are more likely to be optically thin (Kanekar et al. 2021). However, LyC emitters at high redshift exhibit a range of Lyα profiles, including 3–4 peaks (Izotov et al. 2022), single-peaked for Q1549-C25 (Shapley et al. 2016), and absorption rather than emission for Ion1 (Ji et al. 2020). Kerutt et al. (2024) use a larger sample of LyC emitters at $3 < z < 4$ and find no correlation between the Lyα emission and the escape fraction. It is possible that at higher redshifts most ionizing photons escape because of the inhomogeneities in the ISM rather than an optically thin ISM.

4.2. Mergers Driving the LyC Escape

We currently have two models explaining LyC escape: through an optically thin ISM and the picket-fence model (Zackrisson et al. 2013). In the picket-fence model, LyC photons escape through a few optically thin channels in an otherwise optically thick ISM. These channels are typically created by star formation-triggered outflows capable of blowing out neutral gas. LyC emitters in the local Universe often show a significant correlation between the escape fraction and the strength of ionized gas outflows, suggesting that feedback from star formation is responsible for creating these ionized gas channels (Amorín et al. 2024).

However, the mass loading factors for most high-redshift galaxies are similar to those of local dwarf galaxies, even if their SFRs are ten times higher (Concas et al. 2022; Gupta et al. 2022; Carniani et al. 2024; Llerena et al. 2023). Some semi-analytic models of star formation-driven galactic winds suggest that outflowing gas in super star-forming conditions might start radiatively cooling on a relatively short timescale (<1 Gyr, Lochhaas et al. 2018). This rapid cooling might hinder the creation of large-scale channels of optically thin neutral gas solely from star formation alone.

Mergers and galaxy–galaxy interactions are known to tidally strip gas and stars, leading to the formation of highly inhomogeneous galaxies (Toomre & Toomre 1972; Cox et al. 2008; Spilker et al. 2022). Very few LyC emitters in the local Universe are close enough to spatially map their neutral gas density. Deep 21 cm observations on Haro 11, a local LyC emitter, revealed pockets of optically thin neutral hydrogen most likely created by a recent merger event (Le Reste et al. 2024). The large spatial offset (6 kpc) between the peak neutral gas density and the LyC-emitting clump suggests that LyC photons are most likely leaking through these optically thin channels (Le Reste et al. 2024). On the other hand, two other local LyC leakers with 21 cm observations exhibit either only an upper limit on H I mass (Puschnig et al. 2017) or very high gas mass (Haynes et al. 2018), indicating a wide range in the properties of LyC emitters in the local Universe.

Recent work by Gupta et al. (2023) finds that EELGs at $z \sim 3.5$, analogs of galaxies at $z > 6$, are more likely to encounter major mergers and/or strong interactions than typical star-forming galaxies at the same redshift. Other observations (e.g.,Duncan et al. 2019) also find increased merger activity at higher redshifts. For z19863, medium-band images from the FRESCO survey indicate that the galaxy might have experienced a merger recently (Figure 4). Bassett et al. (2018) suggest that the lack of correlation between the O32 ratio and escape fraction could be due to anisotropic neutral gas coverage. In fact, all of their LyC candidates with the lowest O32 ratios showed evidence of disturbed morphology. The peak of Lyα emission for the candidate LyC emitters in Kerutt et al. (2024) is spatially offset by $0\farcs3$–$0\farcs5$ from the peak LyC emission, indicating a mismatch between the peak neutral gas density and ionizing stars. We suspect that inhomogeneities created by a merger event in the neutral ISM might have played a significant role in aiding LyC photons to escape at higher redshifts.

Our observations indicate that in z19863, the ISM is neither optically thin everywhere nor has a complete picket-fence

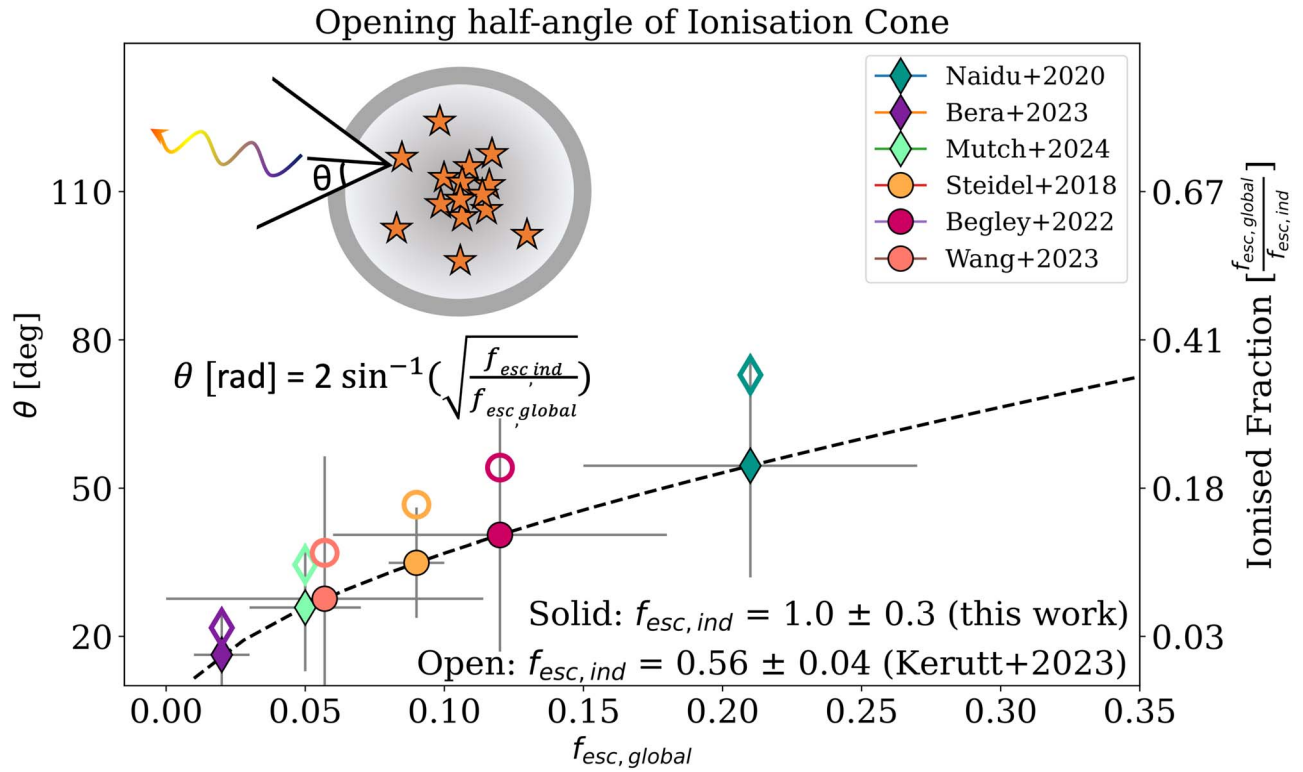

Figure 8. Relation between the opening half-angle of the ionization cone and the global f_{esc} values. The diamonds (purple: Bera et al. 2023, light green: Mutch et al. 2024, dark green: Naidu et al. 2020) and circles (salmon: Wang et al. 2023, yellow: Steidel et al. 2018, magenta: Begley et al. 2022) show the theoretical and observational limits on the global f_{esc} respectively. The solid and open symbols use individual f_{esc} based on z19832 (this work) and average f_{esc} from five gold LyC candidates from Kerutt et al. (2024). The black dashed line is for the fully ionized channels ($f_{esc,ind} = 1$).

structure with many optically thin ionization cones. Here the ISM most likely has a single optically thin ionization cone of neutral ISM created by a recent merger event. The ionizing photons are leaking through this single channel, and by happenstance, its alignment along our line of sight ensures that we can detect the faint signature of ionizing radiation leaking from this single ionization cone.

4.3. Modeling the Opening Angle of Ionizing Channels

If LyC radiation leaks through a few optically thin ionization cones in most galaxies, as it does in z19832, then their random alignment along the line of sight will dictate the number of confirmed detections of LyC emitters. Estimating the total covering fraction of optically thin ISM in high-redshift galaxies is extremely challenging. Lyα photons get fluorescently scattered by neutral hydrogen, and thus a Lyα emission profile provides some hints about the neutral gas density. A small velocity separation and a large ratio of total flux between the blue and red peaks usually indicate an optically thin ISM (Erb et al. 2018; Blaizot et al. 2023; Mukherjee et al. 2023). However, spatially resolving Lyα emission is only possible for a small number of Lyα emitters at $z > 3$, until future spectrographs such as MAVIS (McDermid et al. 2020) become available.

Stacking experiments with large samples of SFGs at $z \sim 3$ have provided some constraints on the average $f_{esc} = 1\%$–10% (Steidel et al. 2018; Wang et al. 2023). Theoretical models using various observations about the reionization history of the Universe, such as neutral gas density, UV luminosity function, etc., constrain the average f_{esc} required (Naidu et al. 2020; Bera et al. 2023; Mutch et al. 2024). However, some individual LyC emitters can have escape fraction as high as 100% (Rivera-Thorsen et al. 2022; Kerutt et al. 2024).

We can use individual f_{esc} measurements to develop a simple model for the total covering fraction or the opening angle of the ionization cone required to reach global f_{esc} values. We assume that all galaxies in the Universe have on average an ionization cone with solid angle Ω and escape fraction $f_{esc,ind}$. The following equation balances the total ionization flux from a single ionization cone with the average escape fraction expected over the entire galaxy ($f_{esc,global}$)

$$\Omega \times f_{esc,ind} = 4\pi \times f_{esc,global}, \implies \Omega = 4\pi \times \frac{f_{esc,global}}{f_{esc,ind}}. \quad (2)$$

For a cone with apex half-angle of θ, the total solid angle is

$$\Omega = 4\pi \sin^2 \frac{\theta}{2}. \quad (3)$$

Therefore, the half-angle of the ionization cone would be

$$\theta[\text{rad}] = 2 \times \sin^{-1} \sqrt{\frac{f_{esc,global}}{f_{esc,ind}}}. \quad (4)$$

Figure 8 shows the average half-angle estimated using Equation (4) based on $f_{esc,ind}$ of z19863 and various measurements of $f_{esc,global}$ from observations (Steidel et al. 2018; Wang et al. 2023) and theory (Naidu et al. 2020; Bera et al. 2023; Mutch et al. 2024). By definition the escape fraction cannot be greater than 1, therefore we assume an absolute escape fraction of 1.00 ± 0.3 rather than the value of $f_{esc}^{abs} = 1.25 \pm 0.3$ estimated in Section 3.2. Additionally, the opening half-angle is

estimated using $f_{\rm esc,ind}$ based on the average escape fraction for the five gold LyC emitter candidates from Kerutt et al. (2024).

Our simple model can help distinguish between more likely measurements of global escape fraction. For instance, if the global escape fraction is constrained to be very low, such as $0.02^{+0.04}_{-0.01}$ (Bera et al. 2023), an ionization cone with an opening half-angle of approximately $\sim16^\circ$ may be sufficient to account for this small escape fraction. Even if only 50% of ionizing photons leak from the ionization cone of most galaxies, the opening half-angle would only need to increase to approximately 23°. This scenario could provide an explanation for the limited number of detections of LyC emitters at higher redshifts. On the other hand, to achieve a global escape fraction of 0.2 (Naidu et al. 2020), ionization cones with $f_{\rm esc,ind} = 1.0$ [$f_{\rm esc,ind} = 0.5$] will need to have an opening half-angle of $\sim53^\circ$ [78°]. Such large opening angles imply that a significant fraction (20%–50%) of the galaxy would need to be leaking ionizing radiation. However, if this were the case, one might expect a larger success rate in building a larger sample of confirmed LyC leakers.

We only need an opening half-angle of $\sim37^\circ$ for a fully ionized cone and $\sim53^\circ$ for an ionization cone with 50% escape fraction to explain the $f_{\rm esc}$ typically observed (Steidel et al. 2018; Wang et al. 2023). As mentioned earlier, observationally determining the opening angle of an ionization cone is very challenging. However, we have some evidence of highly collimated gas outflows in blue compact dwarf galaxies in the local Universe (Herenz et al. 2023). It is worth noting that even at $z = 3$ a partially neutral IGM can absorb a considerable fraction of the ionizing radiation (Bassett et al. 2021), further complicating the detection of LyC emission. Altering the median opening angle of escaping ionizing photons would have an impact on the topology of reionization, and a more sophisticated model would explore the effects of this change on the progress of reionization.

5. Summary

This paper presents discovery of a new candidate LyC emitter (z19863) at $z = 3.088$, where LyC emission is detected using the F336W/UVIS filter on the HST. The galaxy is part of the EELG sample in the MOSEL survey (Tran et al. 2020; Gupta et al. 2022). The LyC emission is spatially offset by $0\farcs29 \pm 0\farcs04 \sim 2.2 \pm 0.3$ kpc from the peak rest-UV emission (F606W). Based on the NIRSpec spectra from JADES, we estimate that the galaxy has low metallicity, high ionization parameter, and low dust attenuation (see Table 1), similar to other LyC emitters at both low and high redshifts.

The deep rest-UV spectrum of the galaxy from the MXDF survey (12 hr integration) exhibit a single-peaked Lyα emission profile and a range of low- and high-ionization absorption features (Figure 7). The lack of rest-UV emission lines such as [O III] 1660, 1666, C IV 1550, [C III] 1907, 1909, etc., which are typically used as proxies for LyC emission (Schaerer et al. 2022), suggests that ISM conditions in this galaxy are dissimilar to those in a typical LyC emitter in the local Universe. Further analyses of the absorption profiles of various species and their correlation with LyC emission (Mauerhofer et al. 2021) is beyond the scope of this paper and will be part of future work.

We hypothesize that LyC photons in z19863 are leaking through a narrow cone of optically thin ISM, likely created by a recent merger event, as indicated by the disturbed morphology in the medium-band imaging (see Section 3.3). The ionization cone is spatially offset by $\sim0\farcs3$ from the nonionizing UV emission and its chance alignment along the line of sight ensures its detection by us. A source similar to z19863 would be missed by studies looking for LyC emission coincident with peak UV emission (e.g., Kerutt et al. 2024). Using a simple toy model, we estimate that the opening half-angle of ionization cones can be as small as 16° to explain some of the global measurements of escape fraction, indicating that a very small fraction of the galaxy needs to be leaking ionizing radiation. Such a small opening angle would also explain the relatively low number of confirmed LyC emitters at high redshifts.

Acknowledgments

This research was supported by the Australian Research Council Centre of Excellence for All Sky Astrophysics in 3 Dimensions (ASTRO 3D), through project number CE170100013. A.A.'s efforts for this work were supported by NSF-AST 1910414.

ORCID iDs

Anshu Gupta https://orcid.org/0000-0002-8984-3666
Cathryn M. Trott https://orcid.org/0000-0001-6324-1766
Ravi Jaiswar https://orcid.org/0000-0003-2035-3850
Ayan Acharyya https://orcid.org/0000-0003-4804-7142
Alex J. Cameron https://orcid.org/0000-0002-0450-7306
Ben Forrest https://orcid.org/0000-0001-6003-0541
Glenn G. Kacprzak https://orcid.org/0000-0003-1362-9302
Themiya Nanayakkara https://orcid.org/0000-0003-2804-0648
Kim-Vy Tran https://orcid.org/0000-0001-9208-2143
Aman Chokshi https://orcid.org/0000-0003-1130-6390

References

Aihara, H., Allende Prieto, C., An, D., et al. 2011, ApJS, 193, 29
Amorín, R. O., Rodríguez-Henríquez, M., Fernández, V., et al. 2024, A&A, 682, L25
Atek, H., Siana, B., Scarlata, C., et al. 2011, ApJ, 743, 121
Bacon, R., Brinchmann, J., Conseil, S., et al. 2023, A&A, 670, A4
Barro, G., Pérez-González, P. G., Cava, A., et al. 2019, ApJS, 243, 22
Bassett, R., Ryan-Weber, E. V., Cooke, J., et al. 2018, MNRAS, 483, 5223
Bassett, R., Ryan-Weber, E. V., Cooke, J., et al. 2021, MNRAS, 502, 108
Begley, R., Cullen, F., McLure, R. J., et al. 2022, MNRAS, 513, 3510
Bera, A., Hassan, S., Smith, A., et al. 2023, ApJ, 959, 2
Bian, F., Fan, X., McGreer, I., Cai, Z., & Jiang, L. 2017, ApJ, 837, L12
Blaizot, J., Garel, T., Verhamme, A., et al. 2023, MNRAS, 523, 3749
Boyett, K., Bunker, A. J., Curtis-Lake, E., et al. 2024, arXiv:2401.16934
Bruzual, G., & Charlot, S. 2003, MNRAS, 344, 1000
Bunker, A. J., Cameron, A. J., Curtis-Lake, E., et al. 2023, arXiv:2306.02467
Cameron, A. J., Saxena, A., Bunker, A. J., et al. 2023, A&A, 677, A115
Cardelli, J. A., Clayton, G. C., & Mathis, J. S. 1989, ApJ, 345, 245
Carniani, S., Venturi, G., & Parlanti, E. 2024, A&A, 685, A99
Charlot, S., & Fall, S. M. 2000, ApJ, 539, 718
Concas, A., Maiolino, R., Curti, M., et al. 2022, MNRAS, 513, 2535
Cox, T. J., Jonsson, P., Somerville, R. S., Primack, J. R., & Dekel, A. 2008, MNRAS, 384, 386
da Cunha, E., Charlot, S., & Elbaz, D. 2008, MNRAS, 388, 1595
da Cunha, E., Walter, F., Smail, I. R., et al. 2015, ApJ, 806, 110
Davis, K., Trump, J. R., Simons, R. C., et al. 2023, arXiv:2312.07799
de Barros, S., Vanzella, E., Amorín, R., et al. 2016, A&A, 585, A51
del Valle-Espinosa, M. G., Sánchez-Janssen, R., Amorín, R., et al. 2023, MNRAS, 522, 2089
Duncan, K., Conselice, C. J., Mundy, C., et al. 2019, ApJ, 876, 110
Eisenstein, D. J., Willott, C., Alberts, S., et al. 2023, arXiv:2306.02465
Eldridge, J. J., Stanway, E. R., Xiao, L., et al. 2017, PASA, 34, e058
Endsley, R., Stark, D. P., Chevallard, J., & Charlot, S. 2020, MNRAS, 500, 5229

Endsley, R., Stark, D. P., Whitler, L., et al. 2023, MNRAS, 533, 1111
Erb, D. K., Steidel, C. C., & Chen, Y. 2018, ApJL, 862, L10
Flury, S. R., Jaskot, A. E., Ferguson, H. C., et al. 2022a, ApJS, 260, 1
Flury, S. R., Jaskot, A. E., Ferguson, H. C., et al. 2022b, ApJ, 930, 126
Forrest, B., Tran, K.-v., Broussard, A., et al. 2018, ApJ, 863, 131
Giacconi, R., Zirm, A., Wang, J., et al. 2002, ApJS, 139, 369
Gordon, K. D., Clayton, G. C., Misselt, K. A., Landolt, A. U., & Wolff, M. J. 2003, ApJ, 594, 279
Gronke, M., & Dijkstra, M. 2016, ApJ, 826, 14
Gupta, A., Jaiswar, R., Rodriguez-Gomez, V., et al. 2023, ApJL, 957, L35
Gupta, A., Tran, K.-V., Mendel, T., et al. 2022, MNRAS, 519, 980
Hainline, K. N., Johnson, B. D., Robertson, B., et al. 2024, ApJ, 964, 71
Haynes, M. P., Giovanelli, R., Kent, B. R., et al. 2018, ApJ, 861, 49
Herenz, E. C., Inoue, J., Salas, H., et al. 2023, A&A, 670, A121
Illingworth, G., Magee, D., Bouwens, R., et al. 2016, arXiv:1606.00841
Inoue, A. K., Shimizu, I., Iwata, I., & Tanaka, M. 2014, MNRAS, 442, 1805
Izotov, Y. I., Chisholm, J., Worseck, G., et al. 2022, MNRAS, 515, 2864
Izotov, Y. I., Orlitová, I., Schaerer, D., et al. 2016a, Natur, 529, 178
Izotov, Y. I., Schaerer, D., Thuan, T. X., et al. 2016b, MNRAS, 461, 3683
Izotov, Y. I., Worseck, G., Schaerer, D., et al. 2018, MNRAS, 478, 4851
Ji, Z., Giavalisco, M., Vanzella, E., et al. 2020, ApJ, 888, 109
Kanekar, N., Ghosh, T., Rhoads, J., et al. 2021, ApJ, 913, L15
Kauffmann, G., Heckman, T. M., Tremonti, C., et al. 2003, MNRAS, 346, 1055
Kennicutt, R. C., Jr., & Evans, N. J., II 2012, ARA&A, 50, 531
Kerutt, J., Oesch, P. A., Wisotzki, L., et al. 2024, A&A, 684, A42
Kewley, L. J., Dopita, M., Sutherland, R. S., Heisler, C., & Trevena, J. 2001, ApJ, 556, 121
Kewley, L. J., Nicholls, D. C., Sutherland, R., et al. 2019, ApJ, 880, 16
Kriek, M., Shapley, A. E., Reddy, N. A., et al. 2015, ApJS, 218, 15
Kumari, N., Amorín, R., Pérez-Montero, E., Vílchez, J., & Maiolino, R. 2021, MNRAS, 508, 1084
Labbé, I., Oesch, P. A., Bouwens, R. J., et al. 2013, ApJ, 777, L19
Lamareille, F., Mouhcine, M., Contini, T., Lewis, I., & Maddox, S. 2004, MNRAS, 350, 396
Le Reste, A., Cannon, J. M., Hayes, M. J., et al. 2024, MNRAS, 528, 757
Leitherer, C., Schaerer, D., Goldader, J. D., et al. 1999, ApJ, 123, 3
Llerena, M., Amorín, R., Pentericci, L., et al. 2023, A&A, 676, A53
Llerena, M., Amorín, R., Pentericci, L., et al. 2024, arXiv:2403.05362
Lochhaas, C., Thompson, T. A., Quataert, E., & Weinberg, D. H. 2018, MNRAS, 481, 1873
Lotz, J. M., Davis, M., Faber, S. M., et al. 2008, ApJ, 672, 177
Lumbreras-Calle, A., López-Sanjuan, C., Sobral, D., et al. 2022, A&A, 668, A60
Mainali, R., Stark, D. P., Tang, M., et al. 2019, MNRAS, 494, 719
Marques-Chaves, R., Schaerer, D., Álvarez-Márquez, J., et al. 2022, MNRAS, 517, 2972
Maseda, M. V., Van Der Wel, A., Rix, H. W., et al. 2014, ApJ, 791, 17
Mauerhofer, V., Verhamme, A., Blaizot, J., et al. 2021, A&A, 646, A80
McDermid, R. M., Cresci, G., Rigaut, F., et al. 2020, Report, Macquarie University
Meštrić, U., Ryan-Weber, E. V., Cooke, J., et al. 2020, MNRAS, 494, 4986
Meštrić, U., Vanzella, E., Upadhyaya, A., et al. 2023, A&A, 673, A50
Mingozzi, M., Belfiore, F., Cresci, G., et al. 2020, A&A, 636, A42
Mukherjee, T., Zafar, T., Nanayakkara, T., et al. 2023, A&A, 680, L5
Mutch, S. J., Greig, B., Qin, Y., Poole, G. B., & Wyithe, J. S. B. 2024, MNRAS, 527, 7924
Naidu, R. P., Tacchella, S., Mason, C. A., et al. 2020, ApJ, 892, 109
Oesch, P. A., Brammer, G., Naidu, R. P., et al. 2023, MNRAS, 525, 2864
Pérez-Montero, E., García-Benito, R., & Vílchez, J. M. 2019, MNRAS, 483, 3322
Popesso, P., Concas, A., Cresci, G., et al. 2022, MNRAS, 519, 1526
Puschnig, J., Hayes, M., Östlin, G., et al. 2017, MNRAS, 469, 3252
Rafelski, M., Teplitz, H. I., Gardner, J. P., et al. 2015, AJ, 150, 31
Ramambason, L., Schaerer, D., Stasińska, G., et al. 2020, A&A, 644, A21
Reddy, N. A., Topping, M. W., Sanders, R. L., Shapley, A. E., & Brammer, G. 2023, ApJ, 948, 83
Rieke, M. & the JADES Collaboration 2023, ApJS, 269, 16
Rinaldi, P., Caputi, K. I., Costantin, L., et al. 2023, ApJ, 952, 143
Rivera-Thorsen, T. E., Dahle, H., Chisholm, J., et al. 2019, Sci, 366, 738
Rivera-Thorsen, T. E., Hayes, M., & Melinder, J. 2022, A&A, 666, A145
Roberts-Borsani, G. W., Bouwens, R. J., Oesch, P. A., et al. 2016, ApJ, 823, 143
Rodriguez-Gomez, V., Snyder, G. F., Lotz, J. M., et al. 2019, MNRAS, 483, 4140
Sanders, R. L., Jones, T., Shapley, A. E., et al. 2019, ApJL, 888, L11
Sanders, R. L., Shapley, A. E., Kriek, M., et al. 2015, ApJ, 816, 23
Saxena, A., Pentericci, L., Ellis, R. S., et al. 2022, MNRAS, 511, 120
Schaerer, D., Izotov, Y. I., Worseck, G., et al. 2022, A&A, 658, L11
Shapley, A. E., Reddy, N. A., Kriek, M., et al. 2014, ApJ, 801, 88
Shapley, A. E., Steidel, C. C., Strom, A. L., et al. 2016, ApJ, 826, L24
Siana, B., Teplitz, H. I., Colbert, J., et al. 2007, ApJ, 668, 62
Spilker, J., Suess, K., Setton, D., et al. 2022, ApJL, 936, L11
Steidel, C. C., Bogosavljević, M., Shapley, A. E., et al. 2018, ApJ, 869, 123
Steidel, C. C., Pettini, M., & Adelberger, K. L. 2001, ApJ, 546, 665
Straatman, C. M. S., Spitler, L. R., Quadri, R. F., et al. 2016, ApJ, 830, 51
Tang, M., Stark, D. P., Chevallard, J., & Charlot, S. 2019, MNRAS, 489, 2572
Tang, M., Stark, D. P., Chen, Z., et al. 2023, MNRAS, 526, 1657
Teplitz, H. I., Rafelski, M., Kurczynski, P., et al. 2013, AJ, 146, 159
Toomre, A., & Toomre, J. 1972, ApJ, 178, 623
Tran, K.-V. H., Forrest, B., Alcorn, L. Y., et al. 2020, ApJ, 898, 45
Vanzella, E., Barros, S. D., Cupani, G., et al. 2016, ApJ, 821, L27
Vanzella, E., Caminha, G. B., Calura, F., et al. 2020, MNRAS, 491, 1093
Vanzella, E., Castellano, M., Bergamini, P., et al. 2022, A&A, 659, A2
Vanzella, E., Giavalisco, M., Inoue, A. K., et al. 2010, ApJ, 725, 1011
Vanzella, E., Guo, Y., Giavalisco, M., et al. 2012, ApJ, 751, 70
Vanzella, E., Nonino, M., Cupani, G., et al. 2018, MNRAS: Letters, 476, L15
Verhamme, A., Orlitová, I., Schaerer, D., & Hayes, M. 2015, A&A, 578, A7
Wang, X., Teplitz, H. I., Smith, B. M., et al. 2023, arXiv:2308.09064
Whitaker, K. E., Ashas, M., Illingworth, G., et al. 2019, ApJS, 244, 16
Williams, C. C., Tacchella, S., Maseda, M. V., et al. 2023, ApJS, 268, 64
Yang, H., Malhotra, S., Gronke, M., et al. 2017b, ApJ, 844, 171
Yang, H., Malhotra, S., Rhoads, J. E., & Wang, J. 2017a, ApJ, 847, 38
Yuma, S., Ouchi, M., Fujimoto, S., Kojima, T., & Sugahara, Y. 2019, ApJ, 882, 17
Zackrisson, E., Inoue, A. K., & Jensen, H. 2013, ApJ, 777, 39